Redox Biology 46 (2021) 102087

Contents lists available at ScienceDirect

Redox Biology

journal homepage: www.elsevier.com/locate/redox

Recruitment and remodeling of peridroplet mitochondria in human adipose tissue

Rebeca Acín-Perez [a,b,1], Anton Petcherski [a,b,1], Michaela Veliova [b,c], Ilan Y. Benador [a,b,d], Essam A. Assali [a,b,e], Georgia Colleluori [f], Saverio Cinti [f], Alexandra J. Brownstein [b,g], Siyouneh Baghdasarian [a,b], Masha J. Livhits [h], Michael W. Yeh [h], Karthickeyan Chella Krishnan [i,j], Laurent Vergnes [b,k], Nathan C. Winn [l,m], Jaume Padilla [l,n], Marc Liesa [a,b,c,g,*], Harold S. Sacks [a,b,o,**], Orian S. Shirihai [a,b,c,d,g,***]

[a] Department of Medicine, Endocrinology, David Geffen School of Medicine, University of California, Los Angeles, CA, 90095, USA
[b] Metabolism Theme, David Geffen School of Medicine, University of California, Los Angeles, CA, 90095, USA
[c] Department of Molecular and Medical Pharmacology, University of California, Los Angeles, CA, 90095, USA
[d] Nutrition and Metabolism, Graduate Medical Sciences, Boston University School of Medicine, Boston, MA, 02118, USA
[e] Department of Clinical Biochemistry, School of Medicine, Ben Gurion University of The Negev, Beer-Sheva, Israel
[f] Department of Experimental and Clinical Medicine, Center of Obesity, Marche Polytechnic University, Ancona, 60020, Italy
[g] Molecular Cellular Integrative Physiology, University of California, Los Angeles, CA, 90095, USA
[h] Section of Endocrine Surgery, David Geffen School of Medicine, University of California, Los Angeles, CA, 90095, USA
[i] Department of Medicine, Division of Cardiology, University of California, Los Angeles, Los Angeles, CA, USA
[j] Department of Pharmacology and Systems Physiology, University of Cincinnati College of Medicine, OH, USA
[k] Department of Human Genetics, David Geffen School of Medicine, University of California, Los Angeles, CA, 90095, USA
[l] Nutrition and Exercise Physiology, University of Missouri, Columbia, MO, USA
[m] Molecular Physiology and Biophysics, Vanderbilt University, Nashville, TN, USA
[n] Dalton Cardiovascular Research Center, University of Missouri, Columbia, MO, USA
[o] Endocrine and Diabetes Division, Veterans Affairs Greater Los Angeles Healthcare System, Los Angeles, CA, USA

ARTICLE INFO

Keywords:
Adipose tissue
Pheochromocytoma
Peridroplet mitochondria
Bioenergetics
Endocrinology

ABSTRACT

Beige adipocyte mitochondria contribute to thermogenesis by uncoupling and by ATP-consuming futile cycles. Since uncoupling may inhibit ATP synthesis, it is expected that expenditure through ATP synthesis is segregated to a disparate population of mitochondria. Recent studies in mouse brown adipocytes identified peridroplet mitochondria (PDM) as having greater ATP synthesis and pyruvate oxidation capacities, while cytoplasmic mitochondria have increased fatty acid oxidation and uncoupling capacities. However, the occurrence of PDM in humans and the processes that result in their expansion have not been elucidated. Here, we describe a novel high-throughput assay to quantify PDM that is successfully applied to white adipose tissue from mice and humans. Using this approach, we found that PDM content varies between white and brown fat in both species. We used adipose tissue from pheochromocytoma (Pheo) patients as a model of white adipose tissue browning, which is characterized by an increase in the capacity for energy expenditure. In contrast with control subjects, PDM content was robustly increased in the periadrenal fat of Pheo patients. Remarkably, bioenergetic changes associated with browning were primarily localized to PDM compared to cytoplasmic mitochondria (CM). PDM isolated from periadrenal fat of Pheo patients had increased ATP-linked respiration, Complex IV content and activity, and maximal respiratory capacity. We found similar changes in a mouse model of re-browning where PDM content in whitened brown adipose tissue was increased upon re-browning induced by decreased housing temperature. Taken together, this study demonstrates the existence of PDM as a separate functional entity in humans and that browning in both mice and humans is associated with a robust expansion of peri-droplet mitochondria characterized by increased ATP synthesis linked respiration.

* Corresponding author. Department of Medicine, Endocrinology, David Geffen School of Medicine, University of California, Los Angeles, CA, 90095, USA.
** Corresponding author. Department of Medicine, Endocrinology, David Geffen School of Medicine, University of California, Los Angeles, CA, 90095, USA.
*** Corresponding author. Department of Medicine, Endocrinology, David Geffen School of Medicine, University of California, Los Angeles, CA, 90095, USA.
E-mail addresses: mliesa@mednet.ucla.edu (M. Liesa), harold.sacks@va.org (H.S. Sacks), oshirihai@mednet.ucla.edu (O.S. Shirihai).
[1] both authors contributed equally.

https://doi.org/10.1016/j.redox.2021.102087
Received 14 June 2021; Received in revised form 21 July 2021; Accepted 27 July 2021
Available online 30 July 2021

1. Introduction

While the majority of adipose tissue in adult humans is white adipose tissue (WAT), brown adipose tissue (BAT) depots and the biogenesis of other thermogenic adipocytes called beige or brite adipocytes are increased under certain conditions [1,2]. Beige and brite adipocytes expend energy through UCP1 mediated uncoupling but also by ATP-consuming futile cycles. Moreover, some studies indicate that energy expenditure involving mitochondrial ATP synthesis and hydrolysis is the primary mechanism behind beige adipocyte thermogenesis. Since uncoupling can inhibit mitochondrial ATP synthesis, it is expected that these two forms of energy expenditure in beige adipocytes are separated to different cells or to different subpopulations of mitochondria inside the same cell, where this ATP-consuming futile cycle could be fueled by ATP-synthesizing mitochondria. Peri-lipid droplet or peridroplet mitochondria (PDM) have been described in mouse BAT, where they were shown to have uniquely high levels of ATP synthesis and lower levels of uncoupling, despite expressing UCP1 [10]. On the other hand, thermogenesis in PDM is thought to be mediated by ATP consuming futile cycles. However, the existence and prevalence of PDM in human white and beige adipocytes have not been determined. The objective of this study is to determine if PDM can be found in human adipose tissue and whether the prevalence of PDM is different in white versus brown adipose tissue and during the process of browning.

Browning occurs in retroperitoneal periadrenal (pADR) adipose tissue in humans with pheochromocytoma (Pheo), an adrenal gland tumor that secretes large amounts of catecholamines [3–7]. pADR adipose tissue browning is characterized by the formation of multilocular, BAT-like, cells, that express UCP1. These BAT-like cells have increased mitochondrial mass as well as respiratory capacity when compared to white adipose tissue that did not undergo browning [8].

We hypothesized that browned white adipose tissue from Pheo patients will harbor a population of lipid droplet-associated mitochondria, which mirror the PDM population that we characterized in mouse BAT. To test this hypothesis, we have isolated and analyzed lipid droplet bound mitochondria from pADR adipose tissue of Pheo patients and compared them to mitochondria derived from both subcutaneous and pADR adipose tissue from control patients [8–10]. As a result, here we determined the bioenergetics of mitochondria interacting with lipid droplets from mouse WAT and BAT, as well as from models of re-browned BAT from obese mice. We extend the characterization to browned white adipose tissue in humans with Pheo and human cervical brown fat. We show that browned white adipose tissue in humans and re-browning of whitened BAT in mice are both associated with an increase in PDM content. Interestingly, we observe that the largest factor contributing to the change in mitochondria bioenergetics in browned human white adipose tissue is an increase in the number of PDM and an elevation of their respiratory activity per unit of PDM. We show for the first time that PDM are a major hallmark of thermogenic adipose tissue deposits in humans and have a conserved function of oxidizing pyruvate and synthesizing ATP in mice and humans.

2. Methods

2.1. Reagents

2.1.1. Human subjects

All human study procedures were approved by the University of California, Los Angeles Institutional Review Board (IRB#13-001332-AM-00005). Details of the study protocol, exclusion criteria, and procedures were published previously [8], except that in this study, retroperitoneal fat adjacent to benign pheochromocytoma tumors or unrelated benign neoplasms was collected prior to rather than after resection of both types of tumor. To ensure no mixing of periadrenal with perirenal fat, care was taken to harvest fat samples from the periadrenal fat avoiding the contiguous fat along the adjacent superior pole of the kidney. Samples of superficial abdominal fat were removed as previously described [8]. Samples were processed for histology, electron microscopy, mitochondrial isolation, protein biochemistry, or snap-frozen in liquid nitrogen [8]. For the study of cervical neck BAT, patients with differentiated thyroid cancer undergoing metastatic neck-lymph node resection and thyroidectomy were consented and ~0.5 g of deep adipose depots, containing BAT, and superficial adipose depots, containing WAT, were collected and processed for histology, electron microscopy, or snap-frozen in liquid nitrogen.

2.2. Blood collection and analysis

Blood from fasting patients was collected preoperatively in EDTA tubes on ice. Whole blood was centrifuged at 900×*g* for 10 min at 4 °C to obtain plasma. Plasma aliquots were sent to Quest Diagnostics to measure the levels of epinephrine, norepinephrine, thyroid-stimulating hormone (TSH), and thyroxine (T4).

2.3. Animals

Twelve-week-old male C57BL6/J mice were used for the isolation of cytoplasmic and peridroplet mitochondria as described previously [10,11]. All animal procedures were executed according to the Guide for Care and Use of Laboratory Animals of the NIH. Mice were fed standard chow (mouse diet 9F, PMI Nutrition International, Brentwood, MO), maintained under controlled conditions (19–22 °C and a 12:12 h light-dark cycle), and all procedures were approved by the Animal Subjects Committee of the University of California, Los Angeles. To evaluate the effects of diet and temperature on PDM, mice were fed one of the following diets: Western diet (WD), 4.73 kcal/g food, 46 % kcal from fat, and 36 % kcal from carbohydrate (17.5 % sucrose and 17.5 % high-fructose corn syrup by weight), and 18 % kcal from protein (modified 58Y1 [5APC]; TestDiet); or control diet (CD), 3.50 kcal/g food, 10 % kcal fat, 72 % kcal carbohydrate, and 18 % kcal protein (58Y2; TestDiet). Mice fed a WD for 9 weeks were either kept under thermoneutral housing conditions (28 °C) or exposed to mild cold (i.e., housed at 20 °C) as described [12]. These procedures were approved by the University of Missouri Institutional Animal Care and Use Committee.

2.4. Histology

Formalin-fixed and paraffin-embedded fat tissues were cut in 4 μm sections and stained with hematoxylin and eosin. Slides were scanned and digitalized using an Aperio AT high-throughput scanner with a 20× air objective and multilocular cell regions were identified by 2–3 independent observers. Four to five 1 mm^2 regions of every section were analyzed for their average lipid droplet size using the Adiposoft plug-in for FIJI/ImageJ filtered for a size range of 1–150 μm [13]. Only subjects where malignant cells were absent on microscopic examination of the fat sections were considered in this study.

2.5. Immunohistochemistry

The expression of UCP1 in fat biopsies was assessed by 3,3′-Diaminobenzidine (DAB) immunohistochemical staining in 4 μm sections with a UCP1 antibody (Abcam, ab10983) at a dilution of 1:500 and hematoxylin as counterstain. Slides were scanned and digitalized using an Aperio AT high-throughput scanner with a 20× air objective. Four to five 1 mm^2 regions of every section were analyzed for UCP1 staining intensity analysis using FIJI/ImageJ.

2.6. Immunofluorescence sample preparation

For Immunofluorescence, 4 μm sections were stained against GRP75 (Antibodies Inc, 75–127 or Abcam ab53098), PLIN1 (Abcam ab61682), and COX4 (Novex 459600) using appropriate secondary antibodies

conjugated to Alexa Fluor 488 (COX4), Alexa Fluor 568 (PLIN1), or Alexa Fluor 647 (GRP75), and DAPI as nuclear stain, as described previously [14].

Whole-mount preparations were generated from small pieces (<5 mm) of formalin-fixed pADR adipose tissue. All staining procedures took place at 4 °C in a reaction tube on a rotating rack. Briefly, tissues were blocked in a solution of PBS, 1 % Triton X-100, 2 % BSA, 5 % normal donkey serum, 0.1 % sodium azide for 2 h, afterwards the solution was replaced with blocking buffer containing antibody against GRP75 for 48 h. Subsequently, tissues were washed 3 times with PBS, 1 % Triton, 30 min per wash, and incubated with a fluorescent conjugated secondary antibody, 1 μg/mL BODIPY493/503 (BD493), and DAPI in blocking buffer for 72–96 h. Following a final wash step, tissues were equilibrated in 70 % glycerol and mounted between two #1.5 glass coverslips separated by a 1 mm deep FastWell™ incubation chamber (Grace Biolabs Inc., Bend, OR) for imaging purposes.

2.7. Peridroplet mitochondria isolation and quantification

All procedures were performed using pre-chilled equipment and solutions. Human samples were collected during surgery in ice-cold PBS. Mitochondria (cytosolic and peridroplet) were isolated using a modification of the protocol described in Refs. [10,11] using a glass/glass homogenizer for human samples and mouse WAT (10 strokes with a loose-fitting and 10 strokes with a tight-fitting pestle) and glass/Teflon for mouse BAT (10 strokes).

The fat layer formed during the low-speed centrifugation step contains lipid droplets and lipid droplet bound mitochondria and is named the pre-stripped fat layer. The floating fat layer formed after high-speed centrifugation includes lipid droplets and no mitochondria and is named the stripped fat layer. The pre-stripped fat layer and the post stripped fat layer were each incubated in MAS (115 mM KCl, 10 mM KH_2PO_4, 2 mM $MgCl_2$, 5 mM HEPES, 1 mM EGTA, 0.1 % BSA) containing Mitotracker deep red (MTDR), (1 μM final) and BODIPY493/503 (1 ng/mL, final) for 10 min at 37 °C to stain mitochondria and lipid, respectively. Unbound dyes were removed by centrifuging the samples at 1000×*g* for 10 min and removing the infranatant below the floating fatty fraction. The stained pre-stripped or stripped fat layers were resuspended in 100 μl of MAS and fluorescence measured in clear-bottom black 96-well plates (Corning) using a Tecan Spark 10 M multimodal plate reader (Tecan Group Ltd., Männedorf, Switzerland). MTDR was excited at 625 nm and its emission recorded at 670 nm. BODIPY493/503 was excited at 488 nm and its emission recorded at 500–550 nm. MTDR/BD493 ratio was calculated from the fluorescence measured in the fat layer and the stripped fat layer. The content of PDM (PDMq) was determined by subtracting the MTDR/BD493 ratio measured in the stripped fat layer (POST centrifugation) from the MTDR/BD493 ratio determined in the fat layer (PRE centrifugation) (Fig. 1A).

2.8. Fluorescence microscopy and image analysis

All fluorescence microscopy was performed using a Zeiss LSM 880 confocal microscope with Airyscan (Carl Zeiss AG, Oberkochen). Fat layers co-stained with MTDR/BD493 were positioned between two #1.5 24 × 50 mm cover glasses, separated by a 0.12 mm imaging spacer (Grace Biolabs), and imaged using a 63X Apochromat oil objective. Whole Mount adipose tissues were imaged using a 40× Apochromat oil objective and IHC-IF sections were imaged using a 100× Apochromat oil objective

Proximity of mitochondrial and lipid droplet staining, as well as mitochondrial COX4 staining intensity, was quantified using CellProfiler 2.0. Briefly, mitochondria located within 500 nm of a PLIN1 positive LD were classified as PDM.

2.9. Respirometry in isolated mitochondria and homogenates

Freshly prepared mitochondria and homogenates were loaded into a Seahorse XF96 microplate in 20 μL of MAS containing substrates. The loaded plate was centrifuged at 2000×*g* for 5 min at 4 °C (no brake) and an additional 130 μL of MAS + GDP (1 mM GDP) was added to each well. To avoid the detachment of mitochondria from the bottom of the plate, MAS was added using a multichannel pipette pointed at a 45° angle to the top of the well-chamber. The final substrate concentrations in the well were: (i) 5 mM pyruvate + 5 mM malate + 4 mM ADP, ii) 5 mM succinate + 2 μM rotenone + 4 mM ADP or (iii) 40 μM palmitoyl-carnitine + 2 mM malate + 4 mM ADP. For pyruvate/ malate and succinate driven respiration; oligomycin was injected in port A (3.5 μM), FCCP in port B (4 μM), N,N,N′,N′-Tetramethyl-p-phenylenediamine (TMPD) + ascorbic acid (0.5 mM + 1 mM) in port C and sodium azide (NaN_3, 50 mM) in port D. For palmitoyl-carnitine dependent respiration; 5 mM malate +4 mM ADP +40 μM palmitoyl-carnitine was injected in port A, oligomycin was injected in port B (3.5 μM), TMPD + ascorbic acid (0.5 mM + 1 mM) in port C and NaN_3 (50 mM) in port D. Mix and measure times were 0.5 min and 4 min respectively. A 2 min wait time was included for respiration measurements after oligomycin injection. Respirometry in previously frozen samples was performed as described [14]. For respiration assays, we loaded 2 μg mouse BAT and WAT mitochondria; 4 μg mouse BAT homogenates; 10 μg mouse WAT homogenates; 4 μg human adipose tissue mitochondria, and 15 μg human adipose tissue homogenate.

2.10. Respirometry studies in whole tissue

10 mg of mouse WAT and BAT were minced into small pieces and placed in an XF24 Islet Capture microplate in 500 μl of assay media (10 mM glucose, 1 mM pyruvate, and 2 mM Glutamine in Seahorse XF assay media). Port injections (final concentration in the well) were as follows: norepinephrine (4 μM) or forskolin (10 μM) in port A; oligomycin (4 μM) in port B and NaN_3 (50 mM) in port C.

2.11. Protein gel electrophoresis and immunoblotting

2.11.1. SDS-PAGE

1–20 μl of fat layer or 10–20 μg protein from total lysates were loaded into 4–12 % Bis-Tris precast gels (ThermoFisher Sci. NP0321) and gel electrophoresis was performed in xCell SureLock Mini-Cells (Novex) under constant voltage of 80 V for 15 min to run through the stacking gel and 120 V for 60 min.

2.12. Immunoblotting

Proteins were transferred to methanol-activated PVDF membrane in xCell SureLock Mini-Cells under 30 V constant voltage for 1 h at 4 °C. Coomassie was washed off of blue native blots using 100 % methanol. Blots were blocked with 3 % BSA in PBST (1 mL/L Tween-20/PBS) and incubated with primary antibody diluted in 1 % BSA/PBST overnight at 4 °C. The next day, blots were washed 3 × 10 min in PBS-Tween, probed with Alexa Fluor 488, IRDye 800CW, or IRDye 680RD conjugated secondary antibodies diluted in blocking solution for 1 h at room temperature, and rinsed again 3 × 10 min in PBST. Detection was achieved using ChemiDoc Molecular Imager (BioRad). Band densitometry was quantified using ImageJ Gel Plugin (NIH). We used the following antibodies: mtOXPHOS cocktail for combined ATP5A, UQCRC2, MTCO1, SDHB, and NUDFB8 detection(Abcam, ab110413), PLIN1 (Abcam, ab61682), UCP1 (Abcam, ab10983), β-actin (Abcam, ab8227), vinculin (Sigma-Aldrich, V9131), and TOMM20 (Santa Cruz Biotechnology, sc-11415).

2.13. Electron microscopy

Mouse tissues were prepared for electron microscopy imaging as previously described [12]. Small pieces of human fat tissue were fixed in 2 % glutaraldehyde, 2 % paraformaldehyde in 0.1 M phosphate buffer, pH 7.4, overnight at room temperature [15]. Subsequently, samples were post-fixed in 1 % osmium tetroxide, dehydrated, and embedded in epoxy resin. Thin sections were cut with an MTX ultramicrotome (RMC, Tucson, AZ), stained with lead citrate, and imaged using a Philips CM10 transmission electron microscope (Philips, Eindhoven, Netherlands) as previously described [10].

2.14. Citrate synthase assay

Assessment of citrate synthase activity was performed as previously described [10] using 1–20 μl of fat layer and stripped fat layer.

2.15. Total glycerol assessment

Fat layer and stripped fat layer (10–15 μl) were incubated in free glycerol reagent buffer (Sigma-Aldrich) containing lipase (40 U/ml, final concentration; EMD Bioscience) in a 96 well plate for 30 min at 37 °C. Absorbance was read at 540 nm. Glycerol standard (Sigma-Aldrich) was used to calculate the amount of glycerol in the samples. Lipase catalyzes the breakdown of triglycerides to fatty acids and glycerol. Determining the amount of total glycerol provides an estimate of total triglyceride content in the sample.

2.16. Principal component analysis (PCA)

A high-dimensional dataset was assembled with data from 17 control and 10 multilocular pheo subjects. We used body mass index (BMI), circulating norepinephrine concentration, PDM content calculated from MTDR/BD493 ratios, and mitochondrial respiration from CM and PDM isolated from SC and pADR adipose tissues. Where necessary, we used the *imputePCA* function from the R *missMDA* package [16] to impute any missing values of our high-dimensional dataset using the principal component analysis method. The percentage of imputed values ranged from 0 to 14.8 % (SD± 5.7 %) with the exception of state 3 respiration under pyruvate and malate and complex IV activity measured by TMPD/ascorbate driven respiration in SC PDM, for which up to 29.6 % of the values had to be imputed. For these specific paramaters of mitochondrial function, imputation was needed given that the isolation of PDM from subcutaneous white adipose tissue had a very low yield that impeded respiratory assays. After imputation, we used the standard *prcomp* function from the built-in R *stats* package to perform PCA to combine the multiple non-independent traits. PCA scores and loadings plots with clustering were constructed using the *autoplot* function from the R *ggfortify* package (https://CRAN.R-project.org/package=ggfortify).

2.17. Statistics

Unless otherwise mentioned in the figure legends, statistical analysis was performed with GraphPad Prism® 9.01 using One-way or Two-way ANOVA. Corrections for multiple comparisons were made by Tukey posthoc test when appropriate. Differences were considered statistically significant at $p < 0.05$. Individual points in a graph denote individual patient samples or biological replicates.

3. Results

3.1. Establishment of a plate reader-based assay for the quantification of peridroplet mitochondria (PDM) using murine samples

Determining the amount of PDM in a quantitative and high-throughput manner is essential to study a large number of phenotypically diverse samples, such as tissues from different human cohorts. The biochemical definition of PDM is based on adherence-to rather than proximity-to lipid droplets (LD). As such, the current method for PDM quantification, electron microscopy, is a suboptimal solution for higher throughput quantification. To develop a biochemical approach to PDM quantification, we employed the concept used for PDM purification from mouse BAT and added new staining steps to label LD and mitochondria with different fluorescent dyes, so that the ratio of lipid content to mitochondria content can be measured. PDM isolation involves centrifugation steps where the fat layer containing mitochondria attached to LD (PDM) is separated first from the rest of mitochondria, named cytosolic mitochondria. To detach PDM from LD, we centrifuged the fat layer at high speed. The fat layer remaining after detaching PDM from LD is referred to as post-stripping fat layer (Fig. 1A). In the fat layer isolated from mouse BAT, we used BODIPY493/503 (BD493) to stain total lipids and evaluated different mitochondrial dyes, with the goal of identifying a dye that will be a reliable reporter for PDM. Comparison of mitochondrial fluorescence dyes indicated that Mitotracker Red CMXROS (MTR) and Mitotracker DeepRed FM (MTDR) both increased in a linear fashion with increasing amounts of BAT fat layer. In comparison, the mitochondrial membrane potential dye TMRE did neither show a linear relationship with the amount of fat layer loaded nor with BD493 signal labeling total lipids (Fig. 1B). In addition, we obtained the same linear relationship when MTDR was used to stain fresh and frozen samples [14], as MTDR binding to mitochondria is less affected by the membrane potential loss due to freezing and thawing (Fig. 1C). Further supporting that MTDR signal is less affected by mitochondrial membrane potential loss, the depolarization induced by FCCP and calcium added to pre-stained isolated mitochondria decreased fluorescence intensity of MTR but not of MTDR (Fig. 1C). To further validate MTDR fluorescence as a measure of mitochondrial mass, we used the same set of samples to determine citrate synthase activity and the content of a series of mitochondrial proteins. Fig. 1D and S1A show the analysis of increasing volumes of BAT fat layer containing mitochondria attached to LDs (pre-stripped fat layer) (Fig. 1D and Fig. S1A). These citrate synthase and Western blot analyses demonstrated a linear correlation between the two additional biochemical markers of mitochondrial content and the amount of BAT fat layer loaded (Fig. 1D and Fig. S1A). Similar results were obtained when gonadal WAT was used instead of BAT (Figs. S1B–D). To validate the lipid quantification assay by BD493, we added a biochemical approach where total lipids are measured by quantifying the glycerol release caused by lipase digestion of triglycerides (Fig. 1E).

We next tested whether our new high-throughput and fluorescence-based PDM quantification assay (HT-PDMA) could detect changes in the attachment of mitochondria to lipid droplets. We previously published that high-speed centrifugation was sufficient to detach mitochondria from the lipid droplet, which was quantified by imaging approaches [10]. Therefore, we used our plate reader and biochemical assays in the fat layer before and after high-speed centrifugation to determine whether these assays could detect the decrease in mitochondria content after centrifugation. Both biochemical and fluorescence-based approaches showed a 50 % reduction in mitochondrial content after high-speed centrifugation (Fig. 1F,G and Figs. S1E–F), which demonstrated the validity and sensitivity of HT-PDMA to detect differences in the mass of mitochondria that are attached to lipid droplets. To test this approach on a physiological model of decreased peridroplet mitochondria (PDM) content, we quantified mitochondria in the fat layer from brown adipose tissue following cold exposure, a treatment previously reported to induce robust detachment of PDM from LDs [10] (Fig. 1H). Our new HT-PDMA and the biochemical assays consistently revealed a decrease in PDM content in cold exposed mice (Fig. 1I and Fig. S1G-H-D), confirming the accuracy of our new fluorescence-based quantification method [10].

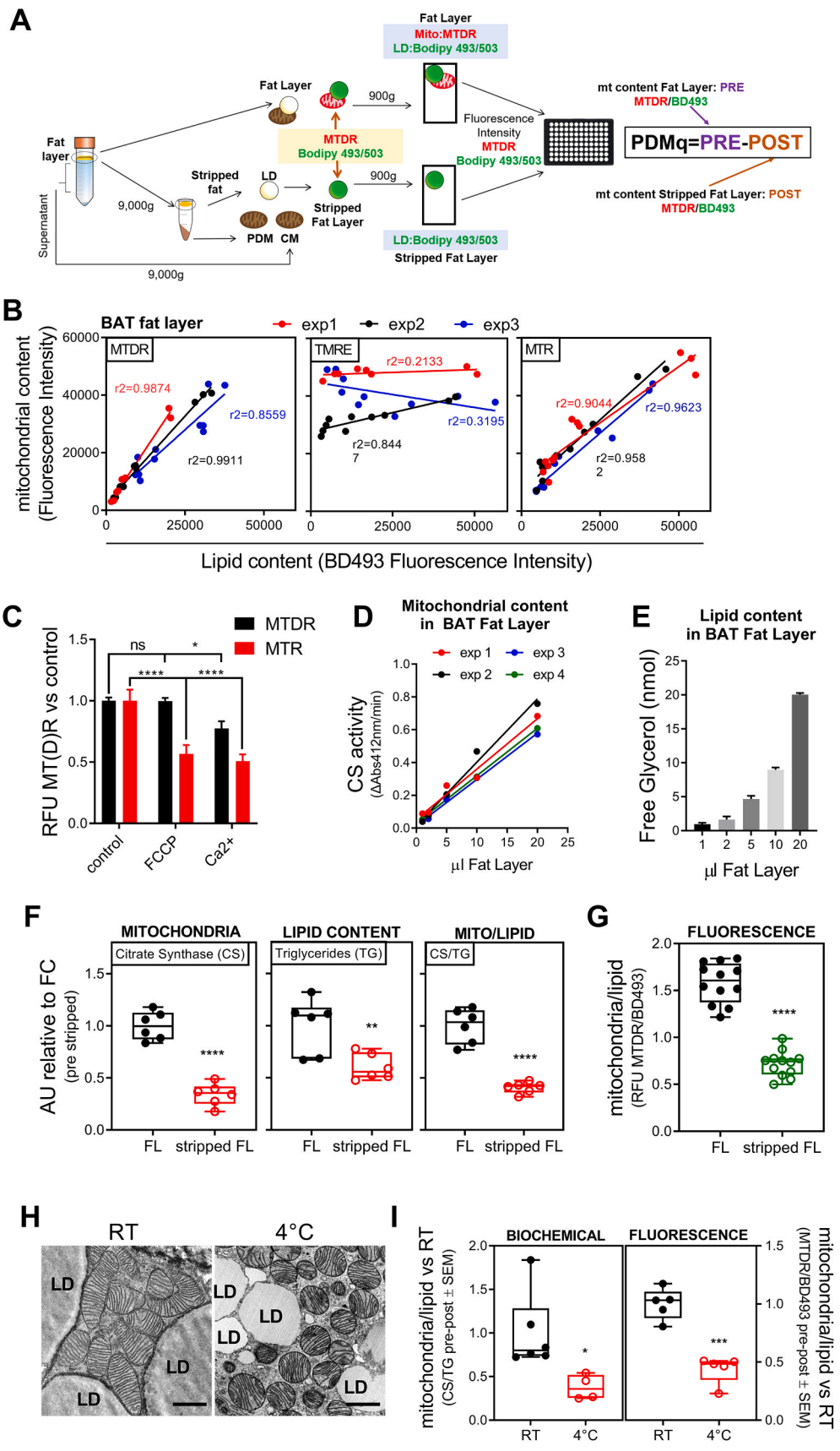

Fig. 1. Isolation and quantification of PDM in murine BAT. A) Scheme illustrating PDM isolation and quantification protocol. B) Fluorescence quantification of lipid and mitochondrial content in BAT fat layer in serial dilution sampling. BOPDIPY493/503 (BD493) was used for lipid staining and TMRE, Mitotracker Red (MTR), and Mitotracker Deep Red (MTDR) were used for mitochondrial staining (n = 3). C) Mitochondria stained with MTR or MTDR in the presence of FCCP and calcium as mitochondrial uncouplers to show staining dependence on membrane potential. MTDR control, MTDR FCCP, n = 18; MTDR Ca^{2+}, n = 6; MTR all conditions, n = 6. D) Mitochondrial activity measured by citrate synthase enzymatic activity at the indicated volume of BAT fat layer (n = 4). E) Total glycerol present in BAT fat layer as an indicator of total fat content (n = 3). F) Mitochondrial (left), lipid (center), and mitochondrial-to-lipid (right) content measured in BAT fat layer and stripped fat layer measured by citrate synthase, total glycerol, and their ratio, respectively (n = 6). G) Mitochondrial-to-lipid fluorescence ratio in BAT fat layer and stripped fat layer (n = 12). H) Transmission electron microscopy from murine BAT at RT and after cold exposure (4 °C). Scale bars are 1 µm. I) PDM quantification using the fluorescence (left) or biochemical (right) method in fat layer from BAT obtained from mice at RT or exposed to cold. In the fluorescence approach: n = 5; in the biochemical approach: RT, n = 6 and 4C, n = 4. *, p < 0.05; **, p < 0.01; ***, p < 0.001; ****, p < 0,0001. (For interpretation of the references to color in this figure legend, the reader is referred to the Web version of this article.)

3.2. Murine white adipose tissue has lower mitochondrial mass and PDM content than brown adipose tissue

Next, we used HT-PDMA to run the first comparative analysis of PDM content in WAT vs BAT. White adipose tissue has lower mitochondrial content than brown adipose tissue, concomitant with lower respiratory activity [17–19]. Indeed, in whole tissue lysates, we found that WAT has reduced levels of mitochondrial respiratory complex subunits, the thermogenic uncoupling protein, UCP1, and the mitochondrial fusion protein, OPA1, as expected (Fig. 2A). Accordingly, quantification of total mitochondrial content by MTDR staining revealed a 50 % decrease in WAT compared to BAT (Fig. 2B). Of note, ATP synthase was the mitochondrial protein showing a milder decrease in WAT when compared to other mitochondrial proteins. Respirometry analysis of BAT and WAT total lysates showed that intact mitochondria from WAT respond to substrates of complex I and complex II, as well as to fatty acids with significantly lower oxygen consumption rates compared to those produced by BAT mitochondria (Fig. 2C and Fig. S2A). Respiration was lower in WAT than in BAT lysates regardless of whether we normalized oxygen consumption either to total mitochondrial content (Fig. 2C) or to whole-cell protein content (microgram of protein), the latter including not only mitochondria but also cytosolic proteins (Fig. S2A). Likewise, WAT samples showed lower respiration driven by complex IV substates TMPD/ascorbate when compared to BAT. This is expected given the lower content of complex IV itself in WAT (Fig. 2C and Fig. S2A). We next quantified respiratory complex activities in permeabilized WAT and BAT mitochondria contained total tissue lysates. Permeabilized mitochondria from BAT had higher oxygen consumption rates as compared to WAT mitochondria under fuels that transfer electrons to complexes I, II, and IV, as predicted by the higher protein content of the different respiratory chain subunits in BAT (Fig. 2D and Fig. S2B). Finally, we measured mitochondrial respiration in intact WAT and BAT, to determine their mitochondrial function in an intact and thus more physiologically relevant context. As predicted based on their different mitochondrial physiology, BAT responded to adrenergic stimulation with both norepinephrine and forskolin by increasing respiration, whereas WAT did not respond (Fig. 2E). Therefore, mitochondrial features observed in total lysates were preserved in intact tissue.

Having characterized the differences in total mitochondrial mass and function in WAT and BAT with our methodologies, we aimed to quantify PDM using our HT-PDMA in parallel to classical biochemical assays in BAT and WAT. Both assays determined a 60–70 % reduction in PDM content in WAT relative to BAT. The same result was obtained when PDM were either normalized to lipid content or total mitochondrial content (Fig. 2F and Fig. S2C). To further confirm HT-PDMA fluorescence-based results, we utilized super-resolution microscopy to directly visualize and quantify PDM attached to lipid droplets from WAT and BAT. High resolution imaging confirmed lower abundance of PDM attached to lipid droplets in WAT when compared to BAT (Fig. 2G). In

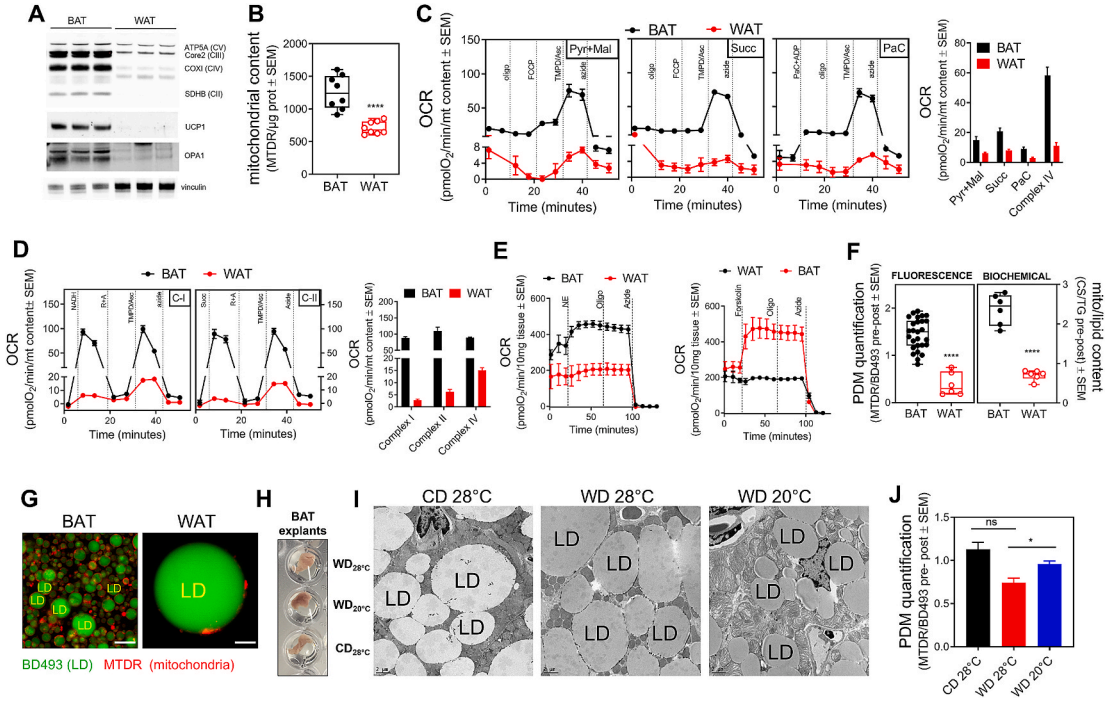

Fig. 2. Mitochondrial bioenergetics differences between different murine adipose tissue depots. A) Representative Western blot of mouse BAT and WAT tissue lysates probed for mitochondrial proteins. B) Mitochondrial content quantification in tissue lysates using MTDR fluorescence method (n = 8). C) Representative respirometry profile and quantification of BAT and WAT tissue lysates respiring upon different substrates (Pyr + Mal, pyruvate plus malate; Succ, succinate plus rotenone; PaC, palmitoyl carnitine plus malate) and complex IV (TMPD/Asc). Oxygen consumption rates (OCR) were normalized to mitochondrial content (n = 5). D) Representative respirometry profile and quantification of BAT and WAT frozen tissue lysates assessing maximal complex I, II, and IV driven respiration. Oxygen consumption rates (OCR) were normalized to mitochondrial content (n = 3). E) Representative respirometry profile in response to norepinephrine (NE) or forskolin of intact BAT and WAT tissue. F) PDM quantification using the fluorescence (left) and biochemical (right) method in WAT and BAT fat layers (Fluorescence: BAT, n = 27; WAT, n = 6; Biochemical: n = 6). G) Representative imaging of WAT and BAT fat layers stained with MTDR (red) and BODIPY493/503 (green). Scale bars are 10 µm. H) BAT explants from mice housed at thermoneutrality (28 °C) and fed either a control diet (CD, appropriate control for the Western Diet) or Western diet (WD) vs. mice exposed to mild cold stress (20 °C) and fed a WD. I) Mitochondrial-lipid juxtaposition by transmission electron microscopy (TEM) in BAT from mice housed at thermoneutrality (28 °C) and fed either a control diet (CD, appropriate control for the Western Diet) or Western diet (WD) vs. mice exposed to mild cold stress (20 °C) and fed a WD (CD 28 °C, n = 6; WD 28 °C, n = 12; WD 20 °C, n = 4). Scale bars are 2 µm. Experimental details were previously reported in Ref. [12]. J) PDM quantification using fluorescence approach in fat layer of BAT from mice housed at thermoneutrality (28 °C) and fed either a CD or WD vs. mice exposed to mild cold stress (20 °C) and fed a WD (CD 28 °C, n = 5: WD 28 °C and WD 20 °C, n = 8). *, $p < 0.05$; ***, $p < 0.001$; ****, $p < 0,0001$. (For interpretation of the references to color in this figure legend, the reader is referred to the Web version of this article.)

all, these data suggest that the major factor determining PDM content is not the size of a lipid droplet, but rather the amount of total mitochondria mass available

With this conclusion, we aimed to test what would occur to PDM recruitment in BAT that had larger lipid droplets. Whitening of BAT is achieved when mice are fed a western diet (WD) under thermoneutrality (28 °C), resulting in increased BAT lipid droplet size and decreased mitochondrial mass, the latter still being higher than in WAT [12]. Following whitening of BAT, re-browning is achieved by moving the mice to a colder temperature (20 °C) [12]. To determine the effect of whitening and re-browning conditions on the abundance of PDM, we quantified PDM using HT-PDMA and validated the results using electron microscopy (Fig. 2H and I). WD-fed mice kept at thermoneutrality showed a reduction in PDM content, which was reversed by subjecting the mice to mild cold-stress (20 °C; re-browning stimulus) while still being fed WD.

3.3. Isolation and characterization of human brown fat from the deep cervical fat depot

Thus far, the existence of PDM as a separate functional entity in humans has not been assessed. To determine the existence of a functional separation between CM and PDM in human brown adipose tissue, we examined deep cervical neck fat depot. Previous studies in humans described active BAT in the neck [5] and cervical region [4–6]. We examined biopsies taken from cancer patients undergoing metastatic neck-lymph node and thyroid resection (Table 2). To assure that tumor cells did not impact the biology of the adipose tissue, we excluded patients with tumor infiltration into the adipose tissue, resulting in the inclusion of a total of 12 patients. We analyzed two different adipose tissue depots from each patient, superficial and deep cervical depots (Fig. S3A). Analysis of H&E staining and UCP1 immunohistochemistry of both depots showed that some deep cervical samples present multilocularity and high UCP1 expression (4 out of 12 patients), a characteristic of BAT, which we referred to as multilocular tissue (multi). In marked contrast, in other patients, this deep cervical depot showed characteristics of WAT, which was referred to as unilocular tissue (uni) (Fig. 3A).

Deep cervical adipose tissue showed higher mitochondrial content, detected both by Western blot and MTDR analysis, and increased maximal mitochondrial respiratory capacity in comparison to *superficial* cervical samples (Fig. 3B–D and Figs. S3B–D). Interestingly, these differences were partially preserved in patients that did not show multilocular adipocytes or UCP1 positive histochemistry. The latter result suggests that small islands of BAT that were outside the sectioning plane can strongly influence the respiratory activity of unilocular adipocytes or that some unilocular adipocytes could have elevated energy expenditure independent of UCP1 activity. Electron microscopy (Fig. 3E) and immunostaining (Fig. 3F) revealed that *deep* cervical fat resembled mouse BAT, showing high mitochondrial density per adipocyte and the presence of mitochondria in close apposition to lipid droplets (PDM).

Table 1
Adrenectomy patient characteristics.

	Control	Pheo	Mann-Whitney test
Numbers*	20	18	
Sex	F [14], M [6]	F [14], M [4]	
Age	51.0±13.7	48.2±21.8	n.s.
BMI	32.0±5.0	26.2±6.7	$p = 0.0012$
Epinephrine (pg/mL)	37.4±27.7	132.8±117.5	$p = 0.0002$
Norepinephrine (pg/mL)	429.8±244.2	4031±5169	$p < 0.0001$
TSH (pg/mL)	1.74±1.0	3.3±1.8	$p = 0.0031$
Free T4 (pg/mL)	1.2±0.3	1.2±0.2	n.s.
Patients with multilocular phenotype	1 (5.0 %)	10 (55.6 %)	

Table 2
Thyroidectomy patient characteristics.

Numbers*	12
Sex	F [9], M [3]
Age	50.4±16.0
BMI	31.2±8.8
Epinephrine (pg/mL)	37.3±21.3
Nor-epinephrine (pg/mL)	623.3±287.6
TSH (pg/mL)	1.7±1.4
Free T4 (pg/mL)	1.3±0.3
Patients with multilocular phenotype	4 (25 %)

*Epinephrine: Control (N = 19), Pheo (N = 14), Thyr. (N = 7); Norepinephrine: Control (N = 20), Pheo (N = 17), Thyr. (N = 6); TSH: Control (N = 19), Pheo (N = 15), Thyr. (N = 11); Free T4: Control (N = 19), Pheo (N = 14), Thyr. (N = 11).

These results confirm that deep cervical adipose depot contains thermogenic adipocytes resembling mouse BAT, as previously suggested [5,6,20]. We next sought to compare the bioenergetic characteristics of CM and PDM in these human cervical depots to those previously characterized in BAT from mice [10]. However, the amount of tissue that was sampled was too small to allow for the isolation of a sufficiently large fat layer from which CM and PDM could be separated and compared. We, therefore, transitioned to the use of periadrenal adipose tissue samples from patients with pheochromocytoma, which develop extensive browning in response to adrenergic stimulation [8].

3.4. Pheochromocytoma patients display browned WAT with high mitochondrial content and respiratory activity

Previous studies demonstrated that 50–60 % of Pheo patients show adipose tissue browning in their periadrenal (pADR) adipose depot adjacent to the tumor. Our study cohort comprised 20 patients with benign unilateral adrenal tumors (controls) and 18 Pheo patients (Table 1). The female-to-male ratio was 14/6 in control patients and 14/4 in Pheo patients. The age range for control patients was 21–72, similar to 18–76 in Pheo patients. Pheo patients consistently displayed a lower BMI at 26 ± 6.7 compared to 32 ± 5 for control patients (Table 1). As published previously, we have classified Pheo patients according to their circulating adrenergic neurotransmitters epinephrine and norepinephrine (Table 1) and pADR depot histological analysis as Pheo unilocular or Pheo multilocular (Fig. 4A) [8]. We focused only on the Pheo multilocular and control subjects, finding multilocular adipocytes only in patients with increased levels of epinephrine, norepinephrine, and thyroid-stimulating hormone (TSH) (Table 1). Despite being associated with high TSH, multilocularity was not correlated to circulating thyroxine (T4) levels. We identified islands of multilocular adipocytes in 55.6 % of pADR fat samples from Pheo patients. In comparison, we did not find any multilocular adipocytes in subcutaneous adipose depots from either control or Pheo patients (Fig. 4A). Multilocular pADR Pheo regions displayed characteristics of browned white adipocytes, including smaller lipid droplet sizes, increased mitochondrial electron transport chain proteins, and UCP1 expression, as revealed by immunocytochemistry and Western blot (Fig. 4B, C, E).

Importantly, our new fluorescence-based plate reader assay (HT-PDMA) detected higher total mitochondrial content in pADR adipose tissue of Pheo patients, measured by MTDR normalized by total protein content, compared to subcutaneous adipose tissue of Pheo patients (Fig. 4D). In control subjects, there was no difference between subcutaneous and pADR adipose tissue. Moreover, by applying *in situ* whole-mount fluorescence microscopy at higher resolution, we observed increased mitochondrial content and smaller lipid droplets in multilocular Pheo adipose cells compared with control patient adipose tissue (Fig. 4F). To analyze respiratory function in these same tissues, we took advantage of the recently published approach for the analysis of respiratory function in frozen tissue homogenates [14]. Compared to control

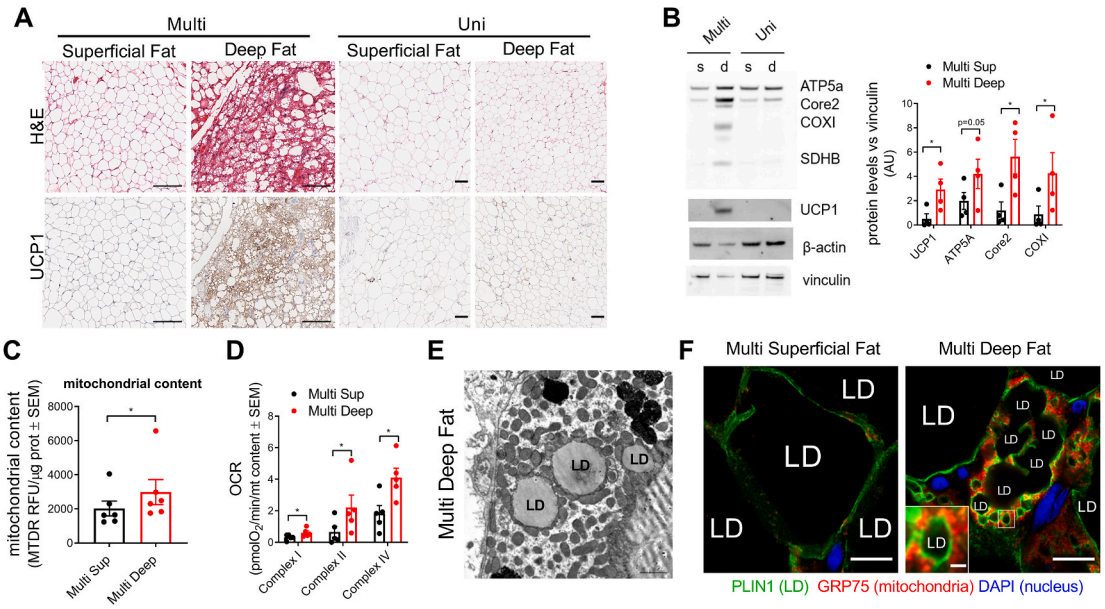

Fig. 3. BAT characteristics of deep cervical human depot. A) Histological H&E staining and UCP1 immunostaining of tissue sections obtained from human superficial and deep cervical fat depots in multi and unilocular patients. Scale bars are 100 µm. B) Representative Western blot of unilocular (Uni) and multilocular (Multi) deep and superficial cervical lysates and quantification of mitochondrial protein levels in the Multi samples (n = 4). C) Mitochondrial content in superficial and multilocular deep cervical fat layer in Multi patients (n = 6). D) Mitochondrial respiration in superficial and multilocular deep cervical frozen lysates in Multi patients (n = 5). E) Representative transmission electron microscopy of cervical deep fat depot from a multi patient. Scale bar = 1000 nm. F) Mitochondrial (GRP75, red), lipid droplet surface (PLIN1, green) immunostaining, and nuclear staining (DAPI, blue) in the indicated samples coming from a multi patient. Scale bars are 10 µm; Scale bar in zoomed insert is 1 µm *, $p < 0.05$ paired Student's t-test. (For interpretation of the references to color in this figure legend, the reader is referred to the Web version of this article.)

patients, Pheo patients had higher levels of complex I, II, and IV–driven respiration rates in their pADR adipose depots, while in SC adipose tissue no differences between control and Pheo patients could be found (Fig. 4G).

3.5. PDM mass and function are increased in browned white adipocytes from Pheochromocytoma patients

To determine if browning is associated with a change in PDM mass and function per PDM, we quantified PDM content in pADR and SC adipose tissue samples from Pheo and control patients, as well as respiratory capacity of isolated PDM. Super-resolution microscopy of formalin-fixed, paraffin-embedded (FFPE) sections stained with antibodies for mitochondrial and LD markers demonstrated higher PDM content in Pheo pADR fat (Fig. 5A). Electron microscopy analysis of multilocular cells in pADR adipose depots of Pheo patients revealed abundant mitochondria-LD contact sites (Fig. 5B). Interestingly, ultrastructural analysis revealed that some patients exhibiting very high levels of circulating norepinephrine [>12000 pg/mL] partially displayed a phenotype of truncated mitochondria and diminished mitochondria-LD contact sites reminiscent of cold-stimulated BAT (Fig. S4).

We have previously shown in mouse BAT that PDM express higher levels of complex IV subunits when compared to cytosolic mitochondria (CM). Super-resolution microscopy analysis of the complex IV subunit COX4 distribution suggests a similar increase in total complex IV content in PDM from human Pheo pADR (Fig. 5C). Using our novel HT-PDMA, we found a 5-6-fold increase in PDM content in the same pADR depot from Pheo patients (Fig. 5D). This is the first evidence that PDM content can be altered in disease. These changes were specific to mitochondria and not to lipid content, since overall lipid droplet content was similar between Pheo and control adipose depots, as measured by protein content of the pan-lipid droplet marker PLIN1 (Fig. 5E) or by total triglyceride content in homogenates (Fig. 5F).

We then proceeded with isolating PDM and CM from different fat depots, using our previously published approach [10,11]. Respirometry analysis revealed elevated state 3 (ATP-synthesizing) respiration driven by complex I substrates in PDM isolated from Pheo pADR when compared to control patients (Fig. 5G). State 3 respiration was also elevated in CM from Pheo pADR compared to control patients although the fold increase was lower than that of PDM (Fig. 5H). Remarkably, we found a large increase in complex IV activity in PDM isolated from Pheo pADR compared to PDM from control patients. In contrast, CM from pADR of Pheo patients showed only a mild increase in complex IV respiration when compared to CM from control patients. These results are consistent with our previously published data that higher complex IV activity is a hallmark of mouse BAT PDM. In striking difference, PDM and CM respiratory function was the same in SC from pADR fat of Pheo patients, as expected given that SC in Pheo patients is not browned. Previous studies in murine BAT found that PDM have a higher capacity to synthesize ATP and oxidize pyruvate and malate, compared to fatty acids [10]. In close resemblance, we find that human PDM also had a higher capacity to oxidize pyruvate and malate, compared to fatty acids (Fig. 5I). These data suggest that a core PDM function, ATP-synthesis driven by pyruvate oxidation, is conserved between mice and humans.

Next, we sought to correlate PDM activity and abundance in pADR tissue with patient characteristics that can potentially predict a whole-body metabolic effect of PDM. To this end, we used principal component analysis (PCA) on 11 non-independent traits to reduce the complexity of the data and to empirically identify patient profiles. The first two principal components, PC1 and PC2, explain about 60 % of the variances (Fig. 5J). Clustering revealed that the samples were tightly grouped together, with no overlap, based on patient groups (control vs. Pheo multilocular). In addition, the first principal component (PC1) is almost completely determined by differences between patient groups and mostly explained by mitochondria-related traits. The loadings plot demonstrated that the difference between the Pheo multilocular and control subjects was largely provided by the higher levels of mitochondria-related traits and lower body mass index (BMI) in the Pheo multilocular group, and *vice versa*. To determine the influence of

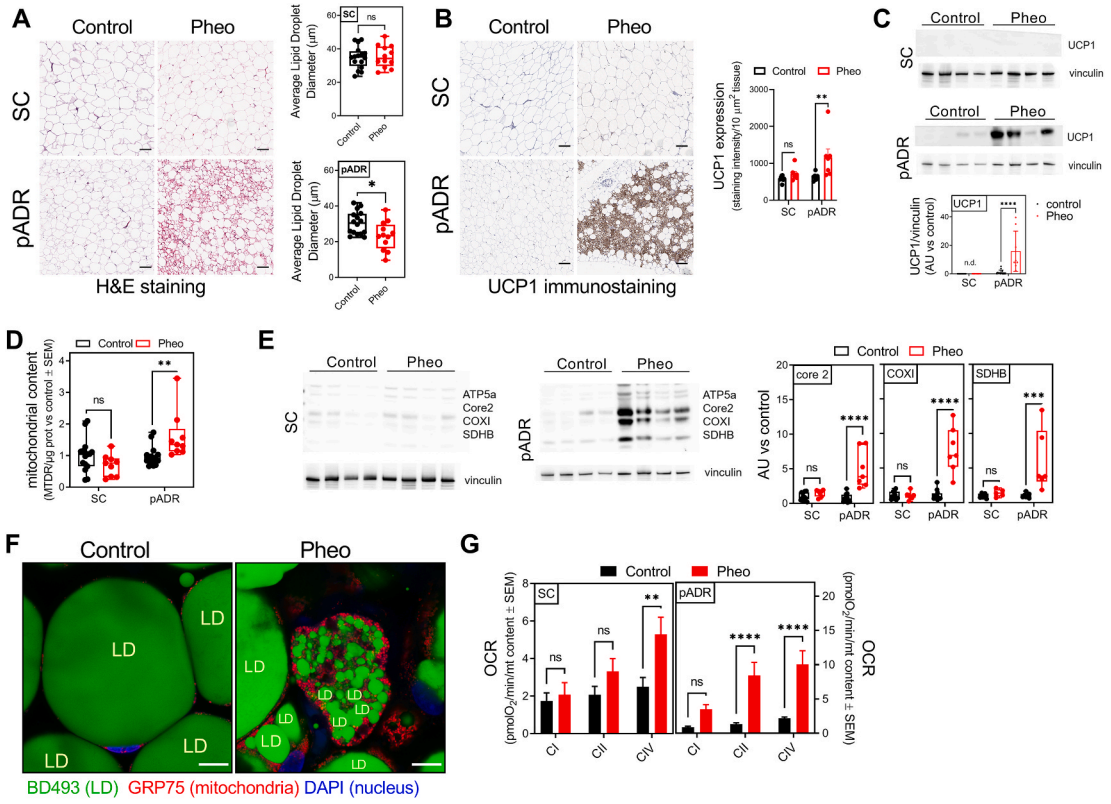

Fig. 4. BAT characteristics of peri-adrenal fat in Pheo patients. A) Histological H&E staining and lipid size quantification of tissue sections obtained from human subcutaneous (SC) and peri-adrenal (pADR) control and Pheo patients (n ≥ 5). Scale bars are 100 μm. B) UCP1 immunostaining and quantification of subcutaneous (SC) and retroperitoneal peri-adrenal (pADR) tissue sections from control and Pheo patients (control, n = 9; Pheo, n = 7). Scale bars = 100 μm. C) Representative Western blot and quantification of UCP1 levels in SC and pADR tissue lysates from control and Pheo patients (control, n = 13; Pheo, n = 8). D) Mitochondrial content in tissue lysates from SC and pADR samples from control and Pheo patients (control, n = 15; Pheo, n = 9). E) Representative Western blot and quantification of mitochondrial respiratory protein levels in SC and pADR tissue lysates from control and Pheo patients (control, n = 12; Pheo, n = 7). F) Representative images of whole mount-periadrenal adipose tissue from control subjects and Pheo patients stained with DAPI (blue), BODIPY493/503 (green), and primary Ab against GRP75 (red). Contrast in the red channel (GRP75) was adjusted to help visualize mitochondrial localization in control samples. Scale bars are 10 μm. G) Mitochondrial respiration in SC and pADR frozen lysates from control and Pheo patients (control, n = 15; Pheo, n = 10). **, p < 0.01; ****, p < 0,0001. (For interpretation of the references to color in this figure legend, the reader is referred to the Web version of this article.)

PDM on Pheochromocytoma, we repeated PCA on PDM- (Fig. 5K) and CM- (Figure 5L) related traits separately. Plotting PDM-related traits separately resulted in PC1 being more strongly determined by the differences between the two groups and the loadings plot demonstrated that this difference was driven by higher levels of PDM-related traits in Pheo multilocular group (Fig. 5K). In contrast, the samples overlapped with each other when we limited the analysis to CM-related traits only (Fig. 5L). Additionally, the loadings plot demonstrated that CM-related traits mostly explained PC2, which is determined by the relative differences among samples within the groups (Fig. 5L). We can conclude that BMI and norepinephrine strongly correlate with the amount and activity of PDM pointing to PDM in adipose tissue as a major driver of browning.

4. Discussion

We have previously shown that peridroplet mitochondria (PDM) in mouse interscapular BAT are a population of mitochondria spatially and functionally distinct from other mitochondria. To date, mitochondrial association with lipid droplets has been demonstrated *in situ* in human tissues in skeletal muscle [21,22], and in primary human adipose tissue explants undergoing a beiging/britening program [23–25]. In this regard, our study is the first attempt to demonstrate that PDM exist as a functionally separated mitochondrial population in human beige adipocytes and white adipose tissue *in situ*. To allow for the comparison of PDM content between different adipose tissues and species, and in response to hormonal triggers, we resorted to a high-throughput approach that does not depend on imaging but instead utilizes fluorescent LD and mitochondrial dyes and a high-throughput capable plate-reader measurement (HT-PDMA). We validated the new approach extensively against an array of biochemical surrogate measurements of mitochondria/LD content, and by modulating PDM content through cold exposure. These experiments confirmed the validity of HT-PDMA as a viable alternative to previous fluorescence or electron microscopy-based methods to quantify PDM. Next, we sought to refine the method through a comparative study of mouse BAT and WAT PDM. We found that in comparison to BAT, WAT has a lower PDM content and the PDM that WAT contains show lower respiratory capacity [12,18,19, 26–30]. Remarkably, BAT whitening in mice was associated with a profound decrease in PDM content, which was restored upon re-browning induced by mild thermal stress. Together, these data demonstrate that PDM content in human WAT and BAT is dynamic, robustly responding to hormonal changes.

In line with previous publications [6,20], we show that deep cervical human adipose depot behaves like active BAT and present new evidence of high PDM content in this tissue.

Browning of the white adipose tissue surrounding the Pheochromocytoma (Pheo) tumor occurs in a high percentage of patients. This browned white adipose tissue can easily be accessed during adrenal tumor resection. It has been shown that perirenal fat from normal subjects contains a heterogeneous collection of dormant preadipocytes that can differentiate into beige multilocular adipocytes, selectively in the

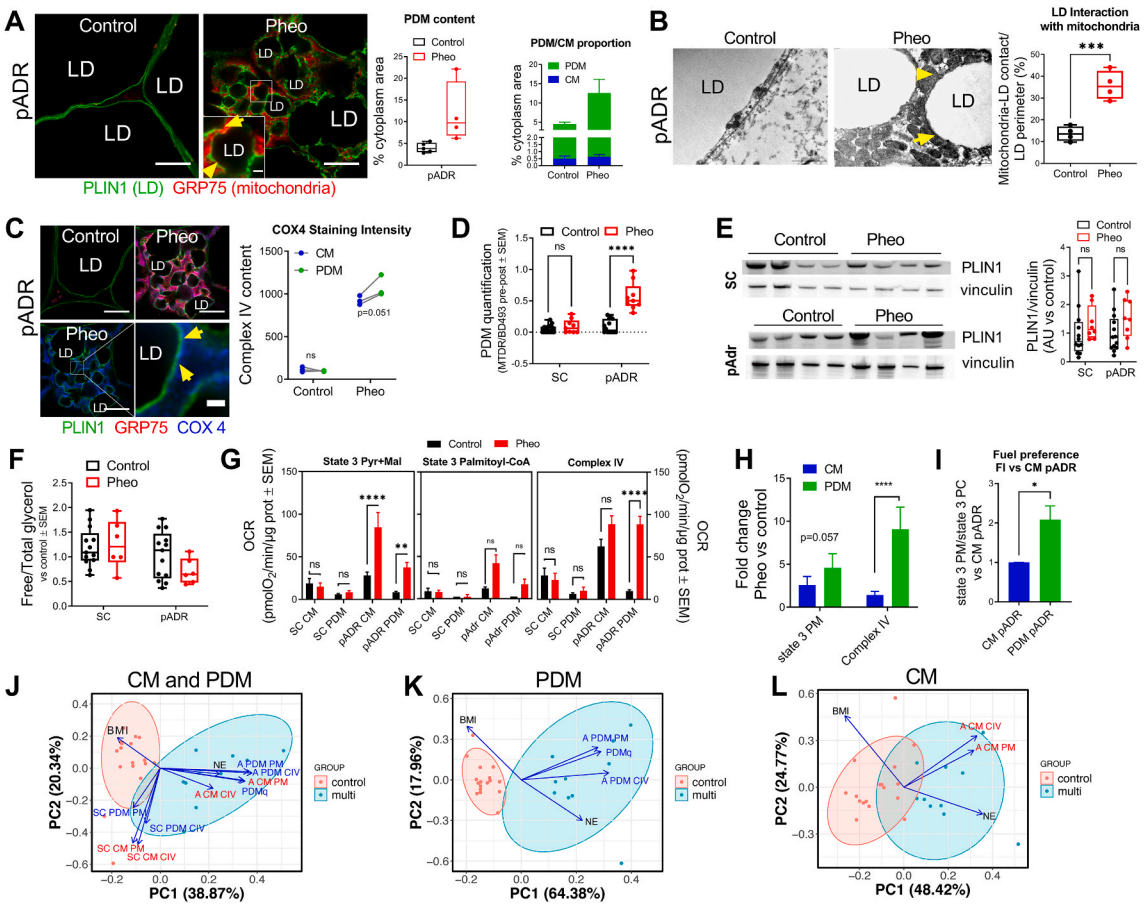

Fig. 5. PDM are present in human fat and share characteristics with murine PDM. A) Immunostaining and image analysis of SC and pADR tissue sections from control and Pheo patients. Mitochondria (GRP75, red) and lipid droplet surface (PLIN1, green) (left). Quantification of the cytoplasm area covered by mitochondria as an indication of PDM content (middle) and calculation of the ratio PDM vs CM (right) (control, n = 5; Pheo, n = 4). Scale bars are 10 µm. Scale bar in zoomed insert is 1 µm. B) Transmission electron microscopy from pADR tissue from control and Pheo patients and quantification of the mitochondrial-lipid juxtaposition relative to the lipid droplet surface (n = 4). Scale bars are 1000 nm. C) Mitochondrial COX4 immunostaining (left) and quantification (right) of pADR tissue sections from control and Pheo patients. Shown are mitochondria (GRP75, red; COX4, blue) and lipid droplet surface (PLIN1, green). COX4 quantification was plotted as a pair to allow comparison between CM and PDM fluorescence intensity within the same sample (n = 3). Scale bars are 10 µm. Scale bar in zoomed panel is 1 µm. A ratio-paired *t*-test was used to determine statistical significance. D) PDM quantification of fat layer in SC and pADR tissue from control and Pheo patients (control, n = 14; Pheo, n = 9). E) Representative Western blot and quantification of Plin1 levels in SC and pADR tissue lysates from control and Pheo (control, n = 13; Pheo, n = 8). F) Measure of total lipid content in SC and pADR lysates from control and Pheo patients (control, n = 13: Pheo, n = 6). G) Pyruvate plus malate driven respirometry driven pyruvate plus malate state 3 (left) and complex IV (right) in CM and PDM from the indicated fat depots in control and Pheo patients (control, n = 15; Pheo n = 7). H–I) Fuel preference in CM and PDM from Pheo patients calculated as the ratio of state 3 from pyruvate plus malate versus palmitoyl-carnitine (H) or the fold increase versus PDM from CM (I) (n = 3). Data from the same Pheo patients in H–I are paired to revealed changes within the same individual. A ratio-paired *t*-test was used to determine statistical significance. J-L) Principal component analysis to determine the influence of peridroplet mitochondria (PDM) on pheochromocytoma. All samples (J), only PDM (K), and only CM (L). In A–C: LD, lipid droplet; yellow arrows indicate PDM. **, $p < 0.01$; ***, $p < 0.001$; ****, $p < 0,0001$. (For interpretation of the references to color in this figure legend, the reader is referred to the Web version of this article.)

superior pole fat adjacent to the adrenal gland. This differentiation to beige has been attributed to their activation by local sympathetic signaling [31], and possibly nor-epinephrine secretion from the adjacent adrenal gland. More than 50 % of our small cohort of Pheo patients had varying levels of multilocular cell islands embedded in the adipose tissue depots of the periadrenal area (pADR). Thus, hypothetically, browned white adipocytes in pADR fat next to pheochromocytomas might result from differentiation of dormant beige cell precursors, mediated by local diffusion of norepinephrine from the tumor into contiguous fat. Mitochondrial content and respiratory capacity, as well as UCP1 expression characteristic of brown/beige adipose tissue, were enhanced in pADR fat from Pheo patients. We found that these exact same samples from Pheo patients showed an increase in PDM content. Pheo PDMs showed an increase in complex IV content and were respiring more actively on pyruvate, recapitulating PDM behavior in mouse BAT.

Beige adipocyte thermogenesis depends on the combination of two energy-consuming processes, uncoupling, and ATP-dependent futile cycles. Depolarization caused by UCP1 activation reduces the production of ATP, the substrate of ATP-dependent futile cycles. On the other hand, PDM are rich in Complex V and ATP produced by PDM could inhibit uncoupling by UCP1 present in PDM. Therefore, for the two processes to function simultaneously, two types of mitochondria are required to co-exist, one that produces heat via UCP1 activation and another that produces ATP. To date, the only co-existing types of mitochondria that fit this description are the PDM and CM. The presence of increased amounts of peri-droplet and cytoplasmic mitochondria in human beige pADR adipose tissue in Pheo patients suggests a division of labor for two key interdependent cellular functions; PDMs mediating ATP formation from glycolysis of glucose to pyruvate for *de novo* droplet triglyceride synthesis, and CMs promoting thermogenesis using non-esterified fatty acids (NEFA) derived from lipid droplet triglyceride (TG) lipolysis. In healthy human adults, the principal source of energy expenditure during cold-stimulated thermogenesis is fatty acid oxidation derived from lipolysis of triglycerides stored in lipid droplets [32].

The decline in triglycerides that accompanies the lipolytic response to cold exposure has been shown to quickly trigger a simultaneous lipogenic response [32,33]. From a teleological perspective, and as suggested by Cannon and Nedergaard, simultaneous activation of lipolysis and lipogenesis might ensure that triglyceride stores are kept replete [34], in anticipation of maintaining core body temperature with further exposure to cold. In this context, PDM may support pyruvate-fueled triglyceride synthesis while at the same time CM may utilize existing TG stores to energize thermogenesis. In addition, PDM can also be supporting energy expenditure via ATP-dependent futile cycles when needed.

This study constitutes the first documentation of the unique functional characteristics of PDM in humans and the first evidence that PDM content can be altered in disease. We further show that human PDM have similar biochemical and bioenergetic characteristics to those described in mice [10]. We show that browning of white adipose tissue in both mice and humans is linked to increases, not only in the abundance of PDM, but also in their bioenergetic capacity per unit of PDM. In addition to their association with browning shown here, PDM were reported to facilitate NEFA esterification to triglycerides, to safely store NEFA in LD [10]. Together these properties of PDM may function to prevent adipose tissue dysfunction characterizing obesity [12,18,19,26–30].

4.1. Limitation of the study

We are aware that our current PDM isolation protocol cannot preclude that there still might be some mitochondria attached to lipid droplets that cannot be stripped using centrifugation. We are currently working on improved methods that will allow for the detachment of the strongly attached mitochondria while preserving their function. This limitation does not change the conclusion that the peridroplet mitochondria isolated by centrifugation have higher ATP synthesizing capacity than non-peridroplet mitochondria.

Declaration of competing interest

The authors declare they have no conflict of interest.

Acknowledgements

The authors would like to acknowledge the Translational Pathology Core Laboratroy at UCLA, Ko Kiehle, Voicu Ciobanu, Ngan Doan, Yunfeng Li, Lauren Orr, Joana Ochoa, and Jennifer Isorena for their technical assistance and Dani Dagan for critical reading of the manuscript and valuable discussion. The authors would like to thank Drs. Karen Reue, Linsey Stiles, Ajit Divakaruni, Barbara Corkey and Mark Prentki for their valuable advice. This work was supported by National Institutes of Health grants U54 DK120342 (LV), NIH-K99DK120875 (KCK), NIH-R00DK120875 (KCK), AHA fellowship 18POST33990256 (KCK), Seed award from DGSOM at UCLA (ML), CURE: DDRC NIH-NIDDK P30 DK041301 (ML), UCLA/UCSD DERC NIH-NIDDK: P30 DK063491 (ML), R01 DK099618-05 (OSS), R01 CA232056-01 (OSS), R21AG060456-01 (OSS), R21 AG063373-01 (OSS), ADA Grant No. 1-19-IBS-049 (OSS), the Cardiometabolic Disease Research Foundation (JP), the Sears Trust Research Foundation (JP), Ministry of Education, University and Research (MIUR).PRIN 2017,#2017L8Z2EM (SC).

Appendix A. Supplementary data

Supplementary data to this article can be found online at https://doi.org/10.1016/j.redox.2021.102087.

Author contributions

Conceptualization, R.A-P, A.P., M.V., I.Y.B., H.S.S., ML and O.S.S.; Methodology, R.A-P, A.P, M.V. and I.Y.B..; Validation, R. A-P., A.P., G. C., K.C.K. and H.S.S. Investigation, R.A-P, A.P., M.V., I.Y.B, E.A., G.C., A. J.B., S.B., K.C.K., N.C.W. J.P., and H.S.S. Human Sample Acquisition, M. J.L, M.W.Y. and H.S.S.; Writing –Original Draft, R.A-P., A.P. and H.S.S.; Writing –Review & Editing, R.A-P., A.P., M.V., I.Y.B., E.A., G.C., S.C., A. J.B., S.B., M.J.L., M.W.Y., L.V., N.C.W., J.P., H.S.S., M.L. and O.S.S.; Funding Acquisition, S.C., M.J.L., M.W.Y., L.V., J.P., M.L. and O.S.S.; Resources, S.C., M.J.L., M.W.Y., L.V., K.C.K., J.P., M.L. and O.S.S. Supervision, R.A-P., A.P., H.S.S., M.L. and O.S.S. All authors read and approved the final version of the manuscript.

References

[1] V. Peirce, S. Carobbio, A. Vidal-Puig, The different shades of fat, Nature 510 (7503) (2014) 76–83.
[2] M. Harms, P. Seale, Brown and beige fat: development, function and therapeutic potential, Nat. Med. 19 (10) (2013) 1252–1263.
[3] M. Giralt, F. Villarroya, White, brown, beige/brite: different adipose cells for different functions? Endocrinology 154 (9) (2013) 2992–3000.
[4] M.E. Lidell, M.J. Betz, O. Dahlqvist Leinhard, M. Heglind, L. Elander, M. Slawik, T. Mussack, D. Nilsson, T. Romu, P. Nuutila, et al., Evidence for two types of brown adipose tissue in humans, Nat. Med. 19 (5) (2013) 631–634.
[5] A.M. Cypess, A.P. White, C. Vernochet, T.J. Schulz, R. Xue, C.A. Sass, T.L. Huang, C. Roberts-Toler, L.S. Weiner, C. Sze, et al., Anatomical localization, gene expression profiling and functional characterization of adult human neck brown fat, Nat. Med. 19 (5) (2013) 635–639.
[6] N.Z. Jespersen, T.J. Larsen, L. Peijs, S. Daugaard, P. Homoe, A. Loft, J. de Jong, N. Mathur, B. Cannon, J. Nedergaard, et al., A classical brown adipose tissue mRNA signature partly overlaps with brite in the supraclavicular region of adult humans, Cell Metabol. 17 (5) (2013) 798–805.
[7] R.B. Iyer, C.C. Guo, N. Perrier, Adrenal pheochromocytoma with surrounding brown fat stimulation, AJR Am. J. Roentgenol. 192 (1) (2009) 300–301.
[8] L. Vergnes, G.R. Davies, J.Y. Lin, M.W. Yeh, M.J. Livhits, A. Harari, M.E. Symonds, H.S. Sacks, K. Reue, Adipocyte browning and higher mitochondrial function in periadrenal but not SC fat in pheochromocytoma, J. Clin. Endocrinol. Metab. 101 (11) (2016) 4440–4448.
[9] A. Frontini, A. Vitali, J. Perugini, I. Murano, C. Romiti, D. Ricquier, M. Guerrieri, S. Cinti, White-to-brown transdifferentiation of omental adipocytes in patients affected by pheochromocytoma, Biochim. Biophys. Acta 1831 (5) (2013) 950–959.
[10] I.Y. Benador, M. Veliova, K. Mahdaviani, A. Petcherski, J.D. Wikstrom, E.A. Assali, R. Acin-Perez, M. Shum, M.F. Oliveira, S. Cinti, et al., Mitochondria bound to lipid droplets have unique bioenergetics, composition, and dynamics that support lipid droplet expansion, Cell Metabol. 27 (4) (2018) 869–885 e6.
[11] J. Ngo, I.Y. Benador, A.J. Brownstein, L. Vergnes, M. Veliova, M. Shum, R. Acin-Perez, K. Reue, O.S. Shirihai, M. Liesa, Isolation and functional analysis of peridroplet mitochondria from murine brown adipose tissue, STAR Protoc 2 (1) (2021) 100243.
[12] N.C. Winn, R. Acin-Perez, M.L. Woodford, S.A. Hansen, M.M. Haney, L.A. Ayedun, R.S. Rector, V.J. Vieira-Potter, O.S. Shirihai, H.S. Sacks, et al., A thermogenic-like Brown adipose tissue phenotype is dispensable for enhanced glucose tolerance in female mice, Diabetes 68 (9) (2019) 1717–1729.
[13] M. Galarraga, J. Campion, A. Munoz-Barrutia, N. Boque, H. Moreno, J.A. Martinez, F. Milagro, C. Ortiz-de-Solorzano, Adiposoft: automated software for the analysis of white adipose tissue cellularity in histological sections, J. Lipid Res. 53 (12) (2012) 2791–2796.
[14] R. Acin-Perez, I.Y. Benador, A. Petcherski, M. Veliova, G.A. Benavides, S. Lagarrigue, A. Caudal, L. Vergnes, A.M. Murphy, G. Karamanlidis, et al., A novel approach to measure mitochondrial respiration in frozen biological samples, EMBO J. (2020), e104073.
[15] S. Cinti, R. Cancello, M.C. Zingaretti, E. Ceresi, R. De Matteis, A. Giordano, J. Himms-Hagen, D. Ricquier, CL316,243 and cold stress induce heterogeneous expression of UCP1 mRNA and protein in rodent brown adipocytes, J. Histochem. Cytochem. 50 (1) (2002) 21–31.
[16] J. Josse, Husson F. missMDA, A package for handling missing values in multivariate data analysis, J. Stat. Software 70 (1) (2016).
[17] M. Veliova, A. Petcherski, M. Liesa, O.S. Shirihai, The biology of lipid droplet-bound mitochondria, Semin. Cell Dev. Biol. 108 (2020) 55–64.
[18] J.H. Lee, A. Park, K.J. Oh, S.C. Lee, W.K. Kim, K.H. Bae, The role of adipose tissue mitochondria: regulation of mitochondrial function for the treatment of metabolic diseases, Int. J. Mol. Sci. 20 (19) (2019).
[19] M. Cedikova, M. Kripnerova, J. Dvorakova, P. Pitule, M. Grundmanova, V. Babuska, D. Mullerova, J. Kuncova, Mitochondria in white, Brown, and beige adipocytes, Stem Cell. Int. 2016 (2016) 6067349.
[20] C. Scheele, T.J. Larsen, S. Nielsen, Novel nuances of human brown fat, Adipocyte 3 (1) (2014) 54–57.
[21] M. Bosma, R. Minnaard, L.M. Sparks, G. Schaart, M. Losen, M.H. de Baets, H. Duimel, S. Kersten, P.E. Bickel, P. Schrauwen, et al., The lipid droplet coat protein perilipin 5 also localizes to muscle mitochondria, Histochem. Cell Biol. 137 (2) (2012) 205–216.
[22] X. Li, Z. Li, M. Zhao, Y. Nie, P. Liu, Y. Zhu, X. Zhang, Skeletal muscle lipid droplets and the athlete's paradox, Cells 8 (3) (2019).

[23] M.J. Lee, S. Jash, J.E.C. Jones, V. Puri, S.K. Fried, Rosiglitazone remodels the lipid droplet and britens human visceral and subcutaneous adipocytes ex vivo, J. Lipid Res. 60 (4) (2019) 856–868.
[24] R. Cereijo, M. Giralt, F. Villarroya, Thermogenic brown and beige/brite adipogenesis in humans, Ann. Med. 47 (2) (2015) 169–177.
[25] D.F. Pisani, V. Barquissau, J.C. Chambard, D. Beuzelin, R.A. Ghandour, M. Giroud, A. Mairal, S. Pagnotta, S. Cinti, D. Langin, et al., Mitochondrial fission is associated with UCP1 activity in human brite/beige adipocytes, Mol. Metab. 7 (2018) 35–44.
[26] P. Illesca, R. Valenzuela, A. Espinosa, F. Echeverria, S. Soto-Alarcon, M. Ortiz, C. Campos, R. Vargas, L.A. Videla, The metabolic dysfunction of white adipose tissue induced in mice by a high-fat diet is abrogated by co-administration of docosahexaenoic acid and hydroxytyrosol, Food Funct. 11 (10) (2020) 9086–9102.
[27] P. Illesca, R. Valenzuela, A. Espinosa, F. Echeverria, S. Soto-Alarcon, C. Campos, A. Rodriguez, R. Vargas, T. Magrone, L.A. Videla, Protective effects of eicosapentaenoic acid plus hydroxytyrosol supplementation against white adipose tissue abnormalities in mice fed a high-fat diet, Molecules 25 (19) (2020).
[28] C.Y. Woo, J.E. Jang, S.E. Lee, E.H. Koh, K.U. Lee, Mitochondrial dysfunction in adipocytes as a primary cause of adipose tissue inflammation, Diabetes Metab. J 43 (3) (2019) 247–256.
[29] J.C. Bournat, C.W. Brown, Mitochondrial dysfunction in obesity, Curr. Opin. Endocrinol. Diabetes Obes. 17 (5) (2010) 446–452.
[30] S. Heinonen, J. Buzkova, M. Muniandy, R. Kaksonen, M. Ollikainen, K. Ismail, A. Hakkarainen, J. Lundbom, N. Lundbom, K. Vuolteenaho, et al., Impaired mitochondrial biogenesis in adipose tissue in acquired obesity, Diabetes 64 (9) (2015) 3135–3145.
[31] N.Z. Jespersen, A. Feizi, E.S. Andersen, S. Heywood, H.B. Hattel, S. Daugaard, L. Peijs, P. Bagi, B. Feldt-Rasmussen, H.S. Schultz, et al., Heterogeneity in the perirenal region of humans suggests presence of dormant brown adipose tissue that contains brown fat precursor cells, Mol. Metab. 24 (2019) 30–43.
[32] V. Ouellet, S.M. Labbe, D.P. Blondin, S. Phoenix, B. Guerin, F. Haman, E. E. Turcotte, D. Richard, A.C. Carpentier, Brown adipose tissue oxidative metabolism contributes to energy expenditure during acute cold exposure in humans, J. Clin. Invest. 122 (2) (2012) 545–552.
[33] D.P. Blondin, S.M. Labbe, H.C. Tingelstad, C. Noll, M. Kunach, S. Phoenix, B. Guerin, E.E. Turcotte, A.C. Carpentier, D. Richard, et al., Increased brown adipose tissue oxidative capacity in cold-acclimated humans, J. Clin. Endocrinol. Metab. 99 (3) (2014) E438–E446.
[34] B. Cannon, J. Nedergaard, Brown adipose tissue: function and physiological significance, Physiol. Rev. 84 (1) (2004) 277–359.